Structural Engineering and Mechanics, Vol. 25, No. 5 (2007) 541-564
DOI: http://dx.doi.org/10.12989/sem.2007.25.5.541

Energy balance and power demand assessment of actuators in base isolated structures supplemented with modified bang-bang control

Robert R. Sebastianelli, Jr.† and Mark A. Austin‡

Department of Civil and Environmental Engineering, and Institute for Systems Research, University of Maryland, College Park, MD 20742, USA

(Received October 12, 2005, Accepted September 19, 2006)

Abstract. This paper investigates the feasibility of supplementing base isolation with active bang-bang control mechanisms. We formulate discrete approximations to energy-balance and power-demand equations for a base isolated structure supplemented with constant stiffness bang-bang (CKBB) control. Numerical experiments are conducted to: (1) Identify situations when constant stiffness bang-bang control is most likely to "add value" to system responses due to base isolation alone, and (2) Quantitatively determine the work done and power required by the actuators. A key observation from the numerical experiments is that "overall performance" of the actuators is coupled to "input energy per unit time."

Keywords: base isolation; bang-bang control; energy-based design.

1. Introduction

To assist engineers in the design of base isolated structures, recent AASHTO and ICBO design codes (AASHTO 1991, ICBO 1997) contain code provisions prescribing a series of standard performance levels for design, together with acceptable levels of structural and non-structural damage, and suggested methods of analysis for performance evaluation. Under minor and moderate earthquake loadings, for example, base isolated structures should suffer no structural damage. For design earthquakes corresponding to the maximum credible ground motion for the site, the main structural members are expected to remain essentially elastic, with nonlinear deformations (i.e., damage) restricted to the isolation devices. Simplified methods of design for base isolated structures have been proposed by Turkington *et al*. (1989a, 1989b), Antriono and Carr (1991a, 1991b), Mayes *et al*. (1992), and Ghobarah and Ali (1990), among others. While these performance-based code provisions and simplified design procedures give high-level guidance regarding acceptable and unacceptable levels of performance (and how to achieve it), there is a mounting body of evidence that base isolation may not always provide adequate protection (Yoshioka 2002). One concern is the possibility of localized buckling of the isolator devices and/or collapse of the structure caused by truly excessive lateral displacements of isolator elements (Naeim and Kelly 1998). A second area of

† Ph.D. Candidate, E-mail: sebastn@umd.edu
‡ Associate Professor, Corresponding author, E-mail: austin@isr.umd.edu.

concern is the inability of base isolation to protect structures against near-source, high-velocity, long-period pulse earthquakes, resulting in excessively large base drifts (Hall *et al*. 1995, Heaton *et al*. 1995, Johnson *et al*. 1998, Spencer *et al*. 2003).

In a first step toward addressing these issues (and potentially achieving a higher level of performance), researchers have proposed systems where the main isolation devices are supplemented by active control mechanisms. Bang-bang control is a natural choice for the implementation of such a system. While numerical algorithms exist for solving the Lyapunov matrix equation, systematic procedures for modeling base isolated structures, supplemented by bang-bang active control are still lacking (Reinhorn *et al*. 1987, Housner and Bergman 1997). As such do we still have a poor understanding of "performance improvements" possible with active components? Similarly, what are the limitations of present-day active component technologies? Answers to these questions are important because of their practical ramifications to design.

2. Objectives and scope

The objectives of this study are two-fold. We seek an analysis procedures that use performance-based metrics (e.g., displacements, velocities, energy) to capture the benefits of active control and base isolation, but are not overly complicated – indeed, we need to keep in mind that the complexity of the design method must be balanced against the uncertainty in ground motion prediction and in modeling of actual structural performance (Austin *et al*. 1987). Energy-balance and power-demand equations are formulated for a base isolated structure supplemented with constant stiffness bang-bang (CKBB) control. While quantitative measurements such as absolute roof acceleration are a good indicator of damage to light internal equipment, occupant discomfort, and other non-structural damage (Kelly and Tsai 1984), energy- and power-balanced based metrics of system performance provide a means for accurately estimating the capacity of a structure to resist forces elastically and dissipate energy associated with damping and key structural elements undergoing cyclic nonlinear deformations. Power-demand analysis extends energy-based analysis to include the external influence and limitations of actuator control on system response.

Numerical experiments are based on time-history responses of a six-DOF nonlinear mass-damping-spring system proportioned according to two design philosophies: (1) Low-damping base isolation (LDBI) for moderate ground motions (i.e., "size and characteristic" of the 1940 El Centro earthquake, PGA~0.35 g), and (2) High-damping base isolation (HDBI) for maximum credible ground motions (e.g., 1994 Northridge earthquake, PGA~1.225 g). For each design philosophy and level of ground shaking, system responses corresponding to base isolation alone serve as a benchmark against which improvements due to active control can be assessed. With this computational framework in place, the specific research objectives of this study are as follows: (1) From energy-balance and power-demand viewpoints, compare the performance of a base isolated building subjected to a variety of actively controlled design criteria and earthquakes, and (2) Compare demands on actuator power to the capabilities of actuator technology. Evaluation of the second objective boils down to a question of technology assessment – can present-day actuator technologies deliver the force/reach implied by the simulations computed in this study?

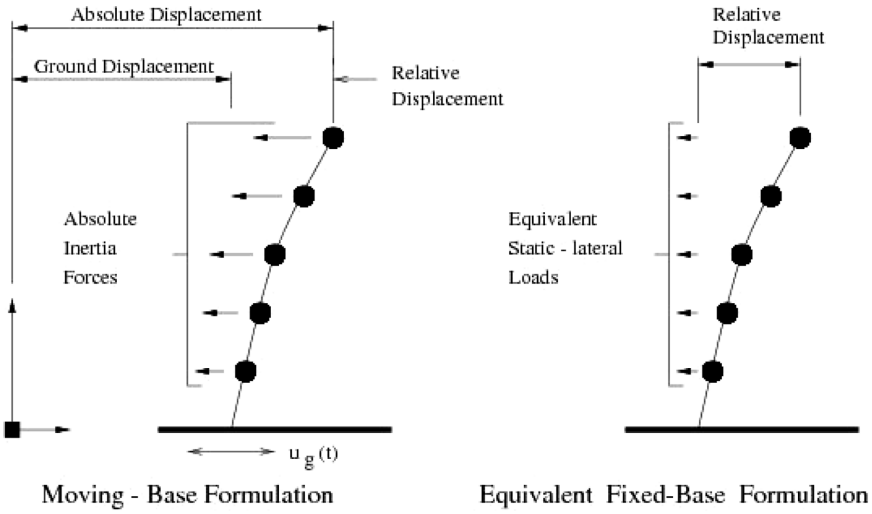

Fig. 1 Moving- and equivalent-base models of system response (forces due to active control not shown)

3. Equations of motion

The left-hand side of Fig. 1 shows the coordinate scheme for dynamics of a multi-degree of freedom structure subject to a horizontal time-varying base motion (actuators not shown). With respect to an absolute coordinate scheme, the equations of equilibrium may be written as a family of n 2nd order differential equations

$$\mathbf{M}\ddot{x}_t(t) + \mathbf{F}(\dot{x}(t), x(t)) = \mathbf{H}u(t) \tag{1}$$

with initial conditions $x_t(0)$ and $\dot{x}_t(0)$. Here $x_t(t) = [x_{1t}(t), x_{2t}(t), \ldots, x_{nt}(t)]^T$ is a $(n \times 1)$ vector of *absolute* system displacements, $\mathbf{M}$ is a $(n \times n)$ mass matrix, and $\mathbf{F}(\dot{x}(t), x(t))$ is a $(n \times 1)$ vector of straining and damping forces depending on displacements and velocities measured *relative* to the base motion. In other words, $\mathbf{F}(\dot{x}(t), x(t)) = \mathbf{F}_{\text{damping}}(\dot{x}(t), x(t)) + \mathbf{F}_{\text{straining}}(\dot{x}(t), x(t))$. $\mathbf{H}$ is an $n \times p$ matrix that designates the location of the controller(s), while $u(t)$ is a p-dimensional vector that represents the control force of p-number of controllers. The relationship between absolute and relative displacements is simply given by

$$x_t(t) = x(t) + rx_g(t) \tag{2}$$

where $x_g(t)$ is the horizontal ground displacement and $\mathbf{r}$ is a $(n \times 1)$ vector describing the movement in each of the structural degrees of freedom due to a unit ground displacement, Substituting Eqs. (2) into (1) and rearranging terms gives

$$\mathbf{M}\ddot{x}(t) + \mathbf{F}(\dot{x}(t), x(t)) = \mathbf{H}u(t) - \mathbf{M}r\ddot{x}_g(t) \tag{3}$$

The right-hand side of Eq. (3) is a vector of equivalent external loads applied at the nodal degrees

of freedom caused by the earthquake ground motions plus, actuator forces applied to the external degrees of freedom. In moving from Eqs. (1) to (3) we are removing the effects of rigid-body displacements from the problem formulation. From a computational standpoint, this is desirable because matrix Eq. (3) may be written entirely in terms of relative displacements (and ground displacements).

When $\mathbf{F}(\dot{x}(t), x(t)) = \mathbf{C}\dot{x}(t) + \mathbf{K}x(t)$, the first-order state-space form of Eq. (3) is as follows

$$\dot{z}(t) = \mathbf{A}z(t) + \mathbf{B}u(t) - \mathbf{W}\ddot{x}_g(t) \tag{4}$$

In Eq. (4), $z(t) = [x(t), \dot{x}(t)]^T$ and

$$\mathbf{A} = \begin{bmatrix} 0 & 1 \\ -\mathbf{M}^{-1}\mathbf{K} & -\mathbf{M}^{-1}\mathbf{C} \end{bmatrix}, \quad \mathbf{B} = \begin{bmatrix} 0 \\ \mathbf{M}^{-1}\mathbf{H} \end{bmatrix} \quad \text{and} \quad \mathbf{W} = \begin{bmatrix} 0 \\ r \end{bmatrix} \tag{5}$$

4. Modified bang-bang control

The control objective for bang-bang control is minimization of the integral

$$J(t) = \frac{1}{2}\int_0^t (z^T(\tau)\mathbf{Q}z(\tau))d\tau \tag{6}$$

where $\mathbf{Q}$ is a positive semi-definite matrix whose content is left for the designer to choose. The well known optimal control solution (Bellman 1956, Wonham and Johnson 1964, Wu and Soong 1996) for a system in the form of Eq. (4) and which minimizes Eq. (6) is

$$u(t) = -U_{\max}\text{sgn}[\mathbf{B}^{\mathbf{T}}\lambda(t)] \tag{7}$$

where $\lambda(t)$ is known as the costate vector that is obtained by solving the following differential equation

$$\dot{\lambda}(t) = -\mathbf{A}^{\mathbf{T}}\lambda(t) - \mathbf{Q}z(t) \tag{8}$$

and $U_{\max}$ is a scalar that represents the maximum actuator control force. To avoid solving Eq. (8) at each time step for the entire time history response, a suboptimal bang-bang control law has been proposed by Wu and Soong (1996). Instead of minimizing Eq. (6), the objective of suboptimal bang-bang control is to minimize the derivative of the following generalized energy function

$$V[z(t)] = z^T(t)\mathbf{S}z(t) \tag{9}$$

Eq. (9) is also referred to as the Lyapunov function, where the $\mathbf{S}$ matrix is the solution to the following Lyapunov matrix equation

$$\mathbf{A}^{\mathbf{T}}\mathbf{S} + \mathbf{S}\mathbf{A} = -\mathbf{Q} \tag{10}$$

Taking the time derivative of Eq. (9) and substituting in the closed-loop state equation leads to the following equation results (Kailath 1980, Wu and Soong 1996)

$$\dot{V}[z(t)] = -z^T(t)\mathbf{Q}z(t) + 2u^T(t)\mathbf{B}^{\mathbf{T}}\mathbf{S}z(t) \tag{11}$$

Close inspection of Eq. (11) indicates that in order for this equation to be a minimum for all possible state variables, $z(t)$, the second term on the right-hand side of Eq. (11) should result in a negative scalar for all possible $z(t)$, and moreover, $u(t)$ must be set to a maximum, say $U_{\max}$. An appropriate choice for $u(t)$ that fulfills these two criteria is

$$u(t) = -U_{\max}\mathrm{sgn}[\mathbf{B}^{\mathbf{T}}\mathbf{S}z(t)] \tag{12}$$

Substituting Eqs. (12) into (3) gives

$$\mathbf{M}\ddot{x}(t) + \mathbf{C}\dot{x}(t) + \mathbf{K}x(t) = -\mathbf{H}U_{\max}\mathrm{sgn}\left[\mathbf{B}^{\mathbf{T}}\mathbf{S}\begin{pmatrix}x(t)\\ \dot{x}(t)\end{pmatrix}\right] - \mathbf{M}r\ddot{x}_g(t) \tag{13}$$

where the matrix, **S**, is the $2n \times 2n$ matrix solution to the Lyapunov matrix equation given in Eq. (10) and **B** is a $2n \times p$ matrix as defined by Eq. (5). The control force, $u(t)$, switches from one extreme to another (i.e., the control force is always exerting its maximum force in either the positive or negative direction). Since the control force always takes on maximum values, the full capabilities of the actuators can be exploited.

4.1 Energy-based bang-bang control

A key tenet of our work is that the terms in **Q** should be selected so that the bang-bang control strategy has a well defined physical meaning, such as minimization of internal energy in the superstructure and isolation devices. Now suppose for the purposes of illustration that we want to apply bang-bang control to the small 2-dof structure in Fig. 2. Assuming that base isolators will be firmly attached to the ground (with full fixity), the integral of internal energy is given by

$$J(t) = \frac{k}{2}\int_0^t (x_1(\tau), x_2(\tau))\begin{bmatrix}1+\gamma & -1\\ -1 & 1\end{bmatrix}\begin{pmatrix}x_1(\tau)\\ x_2(\tau)\end{pmatrix}d\tau \tag{14}$$

where $x_1(\tau)$ and $x_2(\tau)$ are displacements at the nodal degrees of freedom, and k, and γk, are the lateral stiffness in the superstructure and isolation system, respectively. Typically γ will lie in the interval 0.0-0.15. A suitable choice of Q is as follows

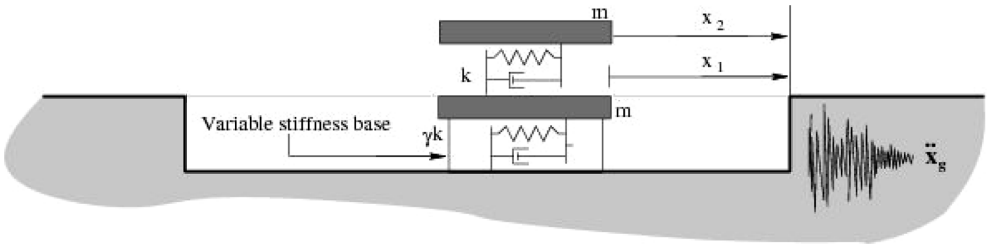

Fig. 2 2-DOF system

$$\mathbf{Q} = \begin{bmatrix} k+\gamma k & -k & 0 & 0 \\ -k & k & 0 & 0 \\ 0 & 0 & 0 & 0 \\ 0 & 0 & 0 & 0 \end{bmatrix} \tag{15}$$

We have recently shown that bang-bang control is insensitive to the nonlinearity of base isolators, and that an elastic or "constant" stiffness may be used to calculate $\mathbf{B}^{\mathbf{T}}\mathbf{S}$ (Sebastianelli and Austin 2005).

5. Foundations for energy-balance calculations

5.1 Formulation of energy-balance equations

Let $\mathbf{R}(\dot{x}(\tau), x(\tau))$ be a force that depends on displacements $x(\tau)$ and velocities $\dot{x}(\tau)$. The work done by $\mathbf{R}(\cdots)$ over the time interval $\tau \in [0, t]$ is denoted $W(t)$, and is given by

$$W(t) = \int_0^t \dot{x}^T(\tau) \cdot \mathbf{R}(\dot{x}(\tau), x(\tau)) d\tau \tag{16}$$

At the highest level of abstraction the energy balance equations can be written

$$\mathbf{W}_{\text{int}}(t) + \mathbf{T}(t) = \mathbf{W}_{\text{act}}(t) + \mathbf{W}_{\text{eq}}(t) = \mathbf{W}_{\text{ext}}(t) \tag{17}$$

where **W**, without subscripts, represents work done and **T** represents kinetic energy. Eq. (17) states that the work done by external loads and actuator forces is converted to kinetic energy and/or internal energy. Energy balance equations have been formulated by Austin and Lin (2003) in both the moving- and fixed-base coordinate frames. Here, we extend that formulation to include the effects of actuator control in the energy-balance assessment.

Substituting Eqs. (1) into (16) and rearranging terms gives

$$\int_0^t \dot{x}^T(\tau)\mathbf{M}\ddot{x}(\tau)d\tau + \int_0^t \dot{x}^T(\tau)\mathbf{F}(\dot{x}(\tau), x(\tau))d\tau = \int_0^t \dot{x}^T(\tau)\mathbf{H}u(\tau)d\tau - \int_0^t \dot{x}^T(\tau)\mathbf{M}r\ddot{x}_g(\tau)d\tau \tag{18}$$

The left-most term represents the work done by nodal inertia forces. The second term represents the work done by internal forces – due to condensation of boundary nodes, internal energy can be expressed in terms of relative displacements and velocities alone. The first term on the right-hand side represents the work done by the actuator forces $\mathbf{H}u(t)$ moving through relative displacements $x(t)$. The right-most term represents work done by equivalent static lateral nodal forces $-\mathbf{M}r\ddot{x}_g(t)$ moving through relative displacements $x(t)$. Integrating the left-most term by parts gives the kinetic energy, $\mathbf{T}(x(t))$, associated with relative displacements alone-it equals the integral of work done by equivalent static lateral node forces over the time interval [0, t].

5.2 Discrete approximation

Discrete approximation of the energy balance equations is necessary when they are being used in

a interactive, time-step analysis. Discrete approximation of the energy balance equations for only the fixed-base (or relative) coordinate frame is considered here. The internal work, $\mathbf{W}_{\text{int}}(t+\Delta t)$, represents the work done by the internal nodal forces moving through the degree of freedom displacements, and is given by

$$\mathbf{W}_{\text{int}}(t+\Delta t) = \mathbf{W}_{\text{int}}(t) + \int_t^{(t+\Delta t)} \dot{\mathbf{W}}_{\text{int}}(\tau)\, d\tau \tag{19}$$

For damped systems, internal nodal forces, $\mathbf{F}_{\text{int}}$, are the sum of damping and straining force components. The rate of internal work is given by

$$\dot{\mathbf{W}}_{\text{int}}(t) = \dot{x}(t)^T \mathbf{F}_{\text{int}}(t) = \dot{x}(t)^T [\mathbf{F}_{\text{straining}}(t) + \mathbf{F}_{\text{damping}}(t)] \tag{20}$$

Substituting Eq. (20) into Eq. (19) and approximating the integral by the trapezoidal rule gives

$$\mathbf{W}_{\text{int}}(t+\Delta t) = \mathbf{W}_{\text{int}}(t) + \frac{\Delta t}{2}(\dot{x}(t)^T \mathbf{F}_{\text{int}}(t) + \dot{x}(t+\Delta t)^T \mathbf{F}_{\text{int}}(t+\Delta t)) \tag{21}$$

The work done by externally applied nodal loads is given by

$$\mathbf{W}_{\text{ext}}(t+\Delta t) = \mathbf{W}_{\text{ext}}(t) + \int_t^{(t+\Delta t)} \dot{\mathbf{W}}_{\text{ext}}(\tau)\, d\tau \tag{22}$$

For the equivalent fixed-base formulation, the rate of work done by earthquake loads is $\dot{W}_{\text{eq}}(t) = -\dot{x}^T(t)\mathbf{M}r\ddot{u}_g(t)$. Approximating Eq. (22) by the trapezoidal rule gives

$$\mathbf{W}_{\text{eq}}(t+\Delta t) = \mathbf{W}_{\text{eq}}(t) + -\frac{\Delta t}{2}(\dot{x}(t)^T \mathbf{M}r\ddot{x}_g(t) + \dot{x}(t+\Delta t)^T \mathbf{M}r\ddot{x}_g(t+\Delta t)) \tag{23}$$

Similarly, the rate of work done by actuator forces is $\dot{W}_{\text{act}}(t) = \dot{x}^T(t)\mathbf{H}u(t)$. Approximating Eq. (22) by the trapezoidal rule gives

$$\mathbf{W}_{\text{act}}(t+\Delta t) = \mathbf{W}_{\text{act}}(t) + \frac{\Delta t}{2}(\dot{x}(t)^T \mathbf{H}u(t) + \dot{x}(t+\Delta t)^T \mathbf{H}u(t+\Delta t)) \tag{24}$$

The kinetic energy at time t is given by

$$\int_0^t \dot{x}^T(\tau)\mathbf{M}\ddot{x}(\tau)\, d\tau = \frac{1}{2}[\dot{x}^T(\tau)\mathbf{M}\dot{x}(\tau)]_0^t = \mathbf{T}(\dot{x}(t)) \tag{25}$$

The actuator power demand is given by

$$\text{Actuator Power } (t) = \left[\frac{W_{\text{act}}(t)}{dt}\right] \approx \left[\frac{W_{\text{act}}(t+\Delta t) - W_{\text{act}}(t-\Delta t)}{2dt}\right] \tag{26}$$

6. Numerical experiments

In this section we employ the Aladdin scripting language (Austin *et al.* 1995, 2000) for a numerical experiment covering the matrix of design cases shown in Fig. 3. The shaded boxes show the two case-study designs: (1) A low damping base isolation (LDBI) system designed to withstand

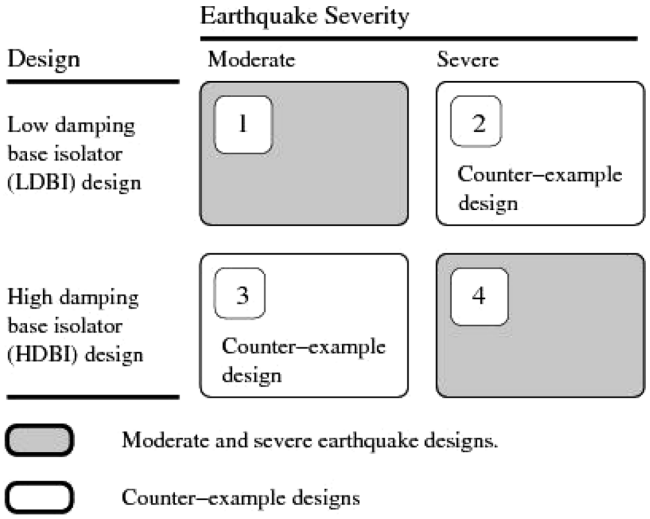

Fig. 3 Scope of case study and counter-example designs covered by the numerical experiments

ground motions of moderate intensity, and (2) A high damping base isolation (HDBI) system designed to withstand ground motions of severe intensity. The unfilled boxes show the two design counter-examples: (1) The LDBI system is subject to a severe earthquake, and (2) The HDBI system is subject to a moderate earthquake. The purpose of the counter examples is to see how CKBB control works seismic events on an unexpected size occur.

For each design case, the numerical computations include work done by the base isolators, superstructure, and actuators, and power required by the actuator. The experimental goal is identification and quantitative evaluation of situations (e.g., moderate versus severe earthquake; expected versus unexpected ground motions) when constant stiffness bang-bang (CKBB) control has the potential for adding significant value to overall performance, compared to base isolation alone. A second experimental goal is assessment of present-day actuator technologies to deliver actuator power requirements estimated through simulation. To quantify improvements in performance due to control, the actively controlled time history responses are benchmarked against corresponding LDBI/HDBI systems responses for base isolation alone.

6.1 Formulation of model

Fig. 4 shows an elevation view of the six-DOF idealized mass-spring-damper model. This model has can be traced back to the work of Ramallo *et al*. (2002) and Kelly *et al*. (1987). Tables 1 and 2 summarize the structural parameters for the low damping base isolator (LDBI) design. For both the LDBI and HDBI designs the mass and damping properties are as shown in Table 1. Table 3 summarizes the structural parameters for the high damping base isolator (HDBI) design. Boundary conditions for the model are full-fixity at the base and full-fixity against vertical displacements and rotations at nodes 2 through 6.

The base isolation element is modeled as a bilinear solid with a force-displacement relationship that follows the kinematic hardening rule. This element was used by Lin (1997) and is a model of a laminated rubber isolator with a lead core. The initial and post-yield shear stiffnesses of the isolator

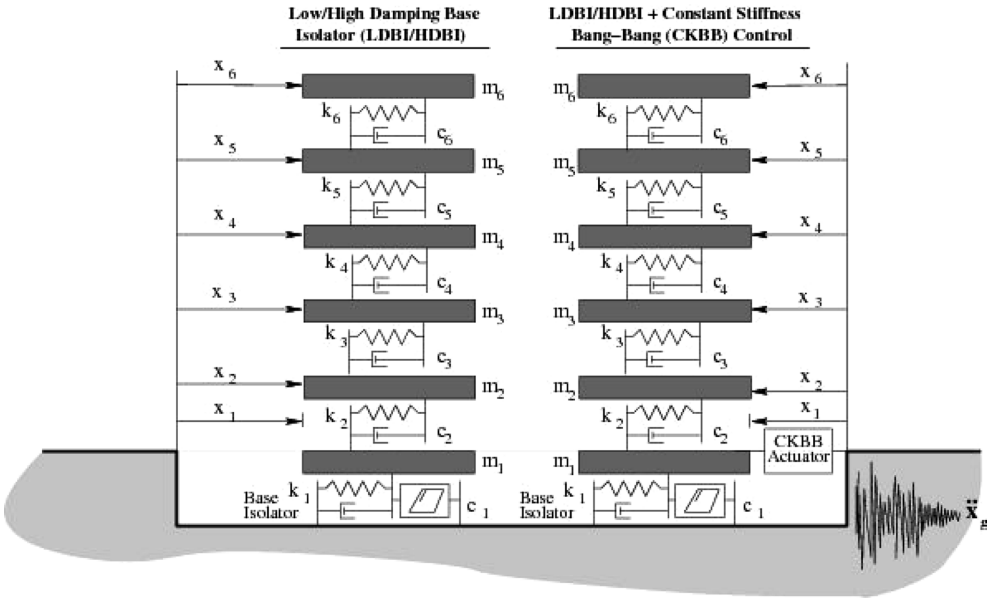

Fig. 4 Elevation view of 6 DOF linear/nonlinear mass-spring-damper system

Table 1 Mass, damping and stiffness properties of Six-DOF mass-spring-damper model with low damping base isolator (LDBI)

	Floor	Damping	Stiffness (kN/m)	
DOF/Mode	Mass (kg)	(kN·s/m)	Pre-yield	Post-yield
1	6,800	3.74	1,392	232
2	5,897	67	33,732	33,732
3	5,897	58	29,093	29,093
4	5,897	57	28,621	28,621
5	5,897	50	24,954	24,954
6	5,897	38	19,059	19,059

Table 2 Natural periods of vibration and modal participation factors for six-DOF mass-spring-damper model: with low damping base isolator (LDBI)

		Period (secs)		Part. factor (Γ)
DOF/Mode	Pre-yield	Post-yield	Pre-yield	Post-yield
1	1.05	2.50	1.05	1.01
2	0.18	0.18	0.06	0.01
3	0.10	0.10	0.01	0.00
4	0.07	0.07	0.01	0.00
5	0.05	0.05	0.00	0.00
6	0.05	0.05	0.00	0.00

are $K_{initial}$ and K_{yield}, respectively. The latter is generated by the stiffness of the rubber, and is fixed at (K_{yield} = 232 kN/m), as to give a post-yield period of 2.5 seconds. Viscous damping from the

Table 3 Properties of six DOF mass-spring-damper model with high damping base isolator (HDBI)

	Stiffness (kN/m)		Period (secs)		Part. factor (Γ)	
DOF/Mode	Pre-yield	Post-yield	Pre-yield	Post-yield	Pre-yield	Post-yield
1	2,320	232	0.83	2.50	1.08	1.01
2	33,732	33,732	0.18	0.18	0.09	0.01
3	29,093	29,093	0.10	0.10	0.02	0.00
4	28,621	28,621	0.07	0.07	0.01	0.00
5	24,954	24,954	0.05	0.05	0.01	0.00
6	19,059	19,059	0.05	0.05	0.00	0.00

rubber is assumed to be 2% critical damping.

6.1.1 Base Isolator (BI) design

Ramallo *et al*. (2002) considers two parameters in the design of the BI, the total yield force, F_y, which is expressed as a fraction of the total structural weight, and the pre-yield to post-yield stiffness ratio of the LRB, $K_{initial}/K_{yield}$. To obtain a post-yield fundamental period of 2.5 seconds, the post-yield stiffness is fixed at $K_{yield} = 232$ kN/m. The body of research supporting the low- and high-damping base isolator design procedures is as follows

1. Low Damping Base Isolator (LDBI). Skinner *et al*. (1993) suggest that for earthquakes having the "severity and character" of El Centro, typical values of the yield force (F_y) should be around 5% of the total structural weight. Park and Otsuka (1999) recommend that F_y range from 4.3 to 5% of the total structural weight for moderate earthquakes (peak ground acceleration (PGA) of 0.35 g). In a third study by Ramallo and co-workers (2002) plots of base drift and structural acceleration as a function of F_y for several values of the stiffness ratio, $K_{initial}/K_{yield}$ were constructed for two- and six-DOF models. The latter study suggests that in order to obtain moderate base drift and acceleration reduction for a ground excitation with PGA = 0.35 g, use $F_y = 5\%$ of the total structural weight and $K_{initial}/K_{yield} = 6$. This low damping base isolation system falls into the "Class (ii): lightly damped" category of Skinner *et al*. (1993).

2. High Damping Base Isolator (HDBI). For severe earthquake events, such as the Kobe and Northridge earthquakes, Ramallo *et al*. (2002) found that in order to obtain significant reductions in base drift and moderate accelerations, isolation device yield strengths and stiffness ratios need to be increased (relative to optimal values for moderate ground motions). Similar observations are reported by Park and Otsuka (1997). They found that for severe ground motion attacks (i.e., PGA of 1.225 g), system performance is best when F_y in the range 14 to 18% of total structural weight.

Hence, in this study, the low damping base isolation (LDBI) design has $F_y = 14.46$ kN (which is 5% of the building weight) and $K_{initial}/K_{yield} = 6$. The LDBI design is typical of low damping isolation systems used in engineering practice, is readily attainable using current technology (Ramallo *et al*. 2002), and follows standard AASHTO code procedures (AASHTO 1991) The high damping base isolator (HDBI) design has a yield force of $F_y = 43.39$ kN = 15% of the building weight and a stiffness ratio of $K_{initial}/K_{yield} = 10$. HDBI designs are not widely used in practice at this time. This may change, however, since there is now significant concern (Hall *et al*. 1995, Heaton *et al*. 1995, Spencer *et al*. 2003) that base isolated buildings may not be able to accommodate severe near-fault earthquakes.

6.1.2 Actuator placement

The scope of this study is restricted to effects of CKBB control for a single actuator positioned at the top of the base isolator (i.e., at degree of freedom 1).

6.1.3 Magnitude of actuator force

In order to provide for a fair comparison between the performance of passive BI damping mechanisms and hybrid LDBI/HDBI+CKBB damping mechanisms, the maximum actuator force ($U_{\max}$) is treated as a design variable. We proceed under the assumption that the LDBI/HDBI+CKBB will not add value to the overall system performance unless the passive and active damping components can work in concert. A number of researchers (e.g., Skinner *et al*. 1993, Wang and Liu 1994, Park and Otsuka 1999, Ramallo *et al*. 2002) have shown that LDBI and HDBI perform well for moderate and servere ground excitations with yield forces, F_y, equal to 5% and 15% of the total weight of the building, respectively. Therefore, for LDBI designs, $U_{\max} = F_y = 14.46$ kN. And for HDBI designs, $U_{\max} = F_y = 43.39$ kN. In all cases, ideal actuator performance is assumed (i.e., the actuator can switch the direction of required forces at high speed, without time delay or actuator dynamics).

6.2 Library of earthquake records

This study employs accelerograms obtained from the Pacific Earthquake Engineering Research (PEER) Center Strong Motion Database (Peer 2004). Ground motions are scaled to moderate and severe intensity.

6.2.1 Moderate ground motion accelerograms

- 1940 El Centro – North-South component of the May 19, 1940, Imperial Valley, CA. USA. earthquake (unscaled magnitude 7.0).
- 1979 El Centro – 3° North-North-West component of the October 15, 1979, Imperial Valley, CA. USA. earthquake (unscaled magnitude 6.5).
- 1987 Whittier – 9° North-North-West component of the October 1, 1987, Whittier, CA. USA. earthquake (unscaled magnitude 6.0).
- 1992 Landers – East-West component of the June 28, 1992, Landers, CA. USA. earthquake (unscaled magnitude 7.3).

The average distance to fault rupture is 11.2 kilometers.

6.2.2 Severe ground motion accelerogram

- 1971 San Fernando – 164° South-South-West component of the February 9, 1971, San Fernando, CA. USA. earthquake (unscaled magnitude 6.6).
- 1994 Northridge – East-West component of the January 17, 1994, Northridge, CA. USA. earthquake (unscaled magnitude 6.7).
- 1995 Kobe – North-South component of the January 16, 1995, Kobe, Japan earthquake (unscaled magnitude 6.9).
- 1999 Duzce – North-South component of the November 12, 1999, Duzce, Turkey earthquake (unscaled magnitude 7.1).

The average distance to fault rupture is 7.3 kilometers.

6.2.3 Ground motion scaling procedure

Individual accelerograms are scaled so that they have approximately the same potential for imparting damage to a structure under moderate and severe ground motion events. The scaling procedure constrains each ground motion to have equal Arias Intensity (Arias 1970) and adjusts the scaling factors so that the average peak ground acceleration has a desired level. Mathematically, if $\ddot{x}_{ig}(t)$ is the i-th ground motion acceleration, then we seek scaling coefficients k_i so that

$$\frac{\pi}{2g}\int_0^{15} k_1^2 \ddot{x}_{1g}^2(\tau)d\tau = \frac{\pi}{2g}\int_0^{15} k_2^2 \ddot{x}_{2g}^2(\tau)d\tau = \ldots = \frac{\pi}{2g}\int_0^{15} k_6^2 \ddot{x}_{6g}^2(\tau)d\tau = \text{constant} \tag{27}$$

The scaled design ground motions were obtained by first isolating the worst fifteen-second sample of each record. Each record was then translated along the y-axis to remove residual velocity effects. Moderate and severe earthquake records were then scaled in the following manner

1. Moderate Earthquake Events. The first group of earthquake records were scaled to an average peak ground acceleration (PGA) of 0.35 g. The Arias Intensity for each scaled record is 1.438 m/sec.

2. Severe Earthquake Events. The second group of earthquake records were scaled to an average PGA of 1.225 g. The Arias Intensity for each scaled record is 12.07 m/sec.

Time histories of Arias Intensity (m/sec) versus time (sec) for the moderate and severe ground motions are shown in Figs. 5 and 6, respectively. Table 4 shows results of the scaling procedures, including the ground motion scaling factor, Arias Intensity, time at which 90% of AI is achieved, PGA, minimum and maximum ground velocities, and the period at which the peak Fourier transform occurs. Average PGA's of 0.35 g and 1.225 g for moderate and severe earthquake events is based on the recommendations of several researchers (Park and Otsuka 1999, Ramallo *et al*. 2002).

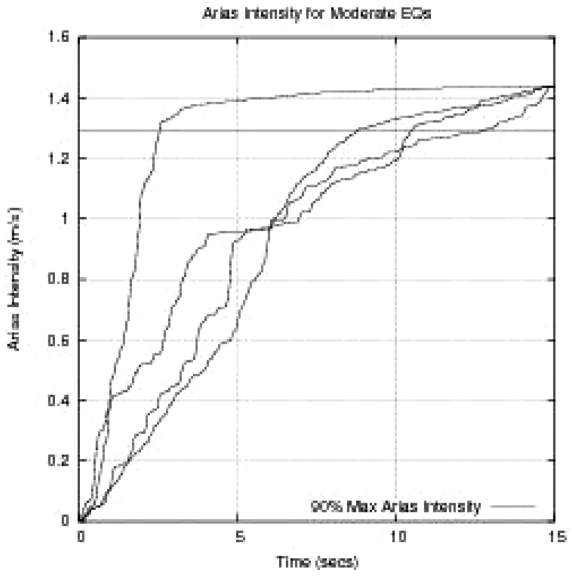

Fig. 5 Arias intensity (m/s) versus time (sec) for moderate ground motions

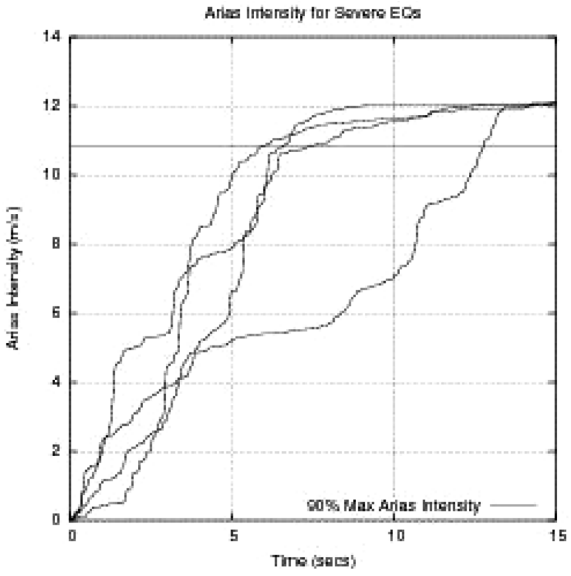

Fig. 6 Arias Intensity (m/s) versus time (sec) for severe ground motions

Table 4 Scaled components of ground motion excitations

Earthquake	Scale Factor	Arias Intensity	Time at 90% AI (secs)	PGA (g)	Velocity (cm/sec) Min.	Velocity (cm/sec) Max.	Fourier Peak (secs)
1940 El Centro	1.031	1.43	10.52	0.323	-17.94	35.64	0.68
1979 El Centro	0.983	1.43	8.78	0.364	-33.60	24.08	0.53
1987 Whittier	1.296	1.43	2.54	0.388	-16.70	28.85	0.29
1992 Landers	1.140	1.43	12.78	0.324	-39.34	26.44	0.75
1971 San Fernando	1.186	12.07	6.62	1.451	-30.69	181.30	0.21
1994 Northridge	0.779	12.07	7.56	1.388	-104.30	44.08	0.35
1995 Kobe	1.205	12.07	6.04	0.989	-100.30	90.27	0.68
1999 Duzce	1.131	12.07	12.78	1.073	-44.34	32.76	0.34

6.3 Duration of performance

The practical implementation of bang-bang control is complicated by the well known problem that during final phases of (low intensity) ground motion, an actuator can actually inject mechanical energy into the structural system, making the system response worse, not better! We circumvent this problem by turning the actuator off when the Arias Intensity for each scaled ground motion input reaches 90% of its final constrained value (i.e., 1.29 m/sec and 10.86 m/sec for moderate and severe earthquakes, respectively). Fig. 7 shows, for example, the time history of actuator force corresponding to the high damping system response generated by the 1971 San Fernando earthquake. The 1971 San Fernando earthquake reaches an Arias Intensity of 10.86 m/sec 6.62 seconds into the time history.

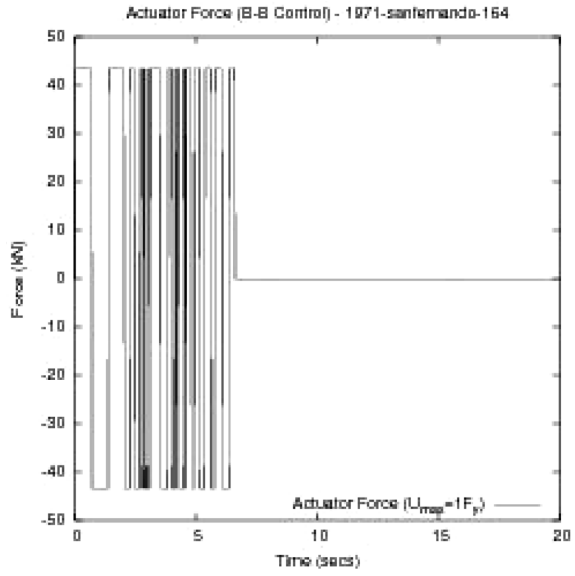

Fig. 7 Actuator time history subjected to 1971 San Fernando

7. Energy balance and power demand assessment

The simulation studies for our scaled 6-DOF model are organized into four practical scenarios

- **Design Case 1.** A moderate severity control design (LDBI and LDBI+CKBB) subjected to a moderate ground excitation (i.e., El Centro characteristic earthquake),
- **Design Case 2.** A moderate severity control design (LDBI and LDBI+CKBB) subjected to a severe ground excitation,
- **Design Case 3.** A high severity control design (HDBI and HDBI+CKBB) subjected to a moderate ground excitation, and
- **Design Case 4.** A high severity design (HDBI and HDBI+CKBB) subjected to a severe ground excitation (i.e., Northridge characteristic earthquake).

Design cases 1 and 4 cover the scenarios of expected ground motion attack. Design cases 2 and 3 are the scenario counter-examples. We expect that by itself, the base isolation system will protect the superstructure by concentrating lateral displacements within the isolator elements. We also expect that the actuator will work to reduce the overall impact of external forces on the base isolated system. This phenomenon is recorded through plots of work done by the actuator (kJ) versus time (sec). A negative slope indicates that the actuator works to extract energy from the external excitations – in other words, negative slopes mean that the actuator is working like a damping mechanism. A positive slope corresponds to energy input.

7.1 LDBI and LDBI+CKBB control subject to moderate ground excitations

The design case 1 scenario corresponds to the system responses generated when LDBI and LDBI+CKBB designs are subject to moderate ground excitations (i.e., average PGA~0.35 g). Table 7 summarizes the peak values of system response generated by four ground motions used in this scenario. In comparing the systems responses for LDBI+CKBB control and LDBI alone, it is evident that for all earthquakes, CKBB control reduces peak values of base drift. The average percentage of base drift reduction is 44%. Reductions in peak values of base drift are accompanied by marginal increases in the peak structural drift. In all cases, however, the magnitude of peak drifts in the isolator is much larger than in the superstructure (i.e., the isolator system is working the way it's supposed to!). CKBB control also affects the work done by the base isolator and superstructure. For all earthquake inputs, adding control decreases the work done by the base isolator. However, adding control decreases the work done by the superstructure in only half of the system responses. The average value of work done by the actuator is 7.08 kJ. The average value of power requirements is 5.63 kW.

7.2 LDBI and LDBI+CKBB control subject to severe ground excitations

The design case 2 scenario corresponds to system responses generated when LDBI and LDBI+CKBB designs are subject to unexpectedly severe, yet conceivable, ground motions (i.e., PGA~1.225 g). Table 7 summarizes the peak values of system response generated by the four ground motions used in this scenario. With the exception of the 1999 Duzce case study, the peak values of base drift were reduced with the addition of CKBB control. On average, peak base drifts are reduced by 11%. Peak values of structural drift were virtually unchanged, except for the 1999

Table 5 Design Case 1. Peak values of system response for LDBI and LDBI+CKBB subjected to moderate ground motions

	Base		Structural		Isolator		Structural		Actuator	Actuator
	Drift (mm)		Drift (mm)		Work (kJ)		Work(kJ)		Work (kJ)	Power (kW)
		LDBI+		LDBI+		LDBI+		LDBI+	LDBI+	LDBI+
Earthquake	LDBI	CKBB	LDBI	CKBB	LDBI	CKBB	LDBI	CKBB	CKBB	CKBB
1940 El Centro	79.8	45.89	0.77	1.88	10.44	6.91	2.33	2.42	−8.46	5.68
1979 El Centro	155.8	68.03	1.22	1.74	14.28	4.34	4.43	2.37	−4.19	5.45
1987 Whittier	72.6	33.50	0.74	1.64	2.35	1.48	1.32	2.12	−2.90	4.70
1992 Landers	162.3	125.90	1.25	1.77	20.21	11.14	6.05	3.49	−12.78	6.67
Average value:	117.6	68.33	0.99	1.75	11.82	5.96	3.53	2.60	−7.08	5.62

Table 6 Design Case 2. Peak values of system response for LDBI and LDBI+CKBB subjected to severe ground motions

	Base		Structural		Isolator		Structural		Actuator	Actuator
	Drift (mm)		Drift (mm)		Work (kJ)		Work (kJ)		Work (kJ)	Power (kW)
		LDBI+		LDBI+		LDBI+		LDBI+	LDBI+	LDBI+
Earthquake	LDBI	CKBB	LDBI	CKBB	LDBI	CKBB	LDBI	CKBB	CKBB	CKBB
1971 San Fernando	529.8	454.50	3.26	3.26	59.27	45.77	52.08	41.48	−37.96	24.27
1994 Northridge	238.8	211.00	1.79	1.92	21.17	17.81	12.27	12.13	−18.88	12.87
1995 Kobe	354.6	251.50	2.36	2.19	49.69	42.33	38.93	26.93	−33.86	18.65
1999 Duzce	39.2	43.02	0.80	2.41	5.16	4.44	3.01	4.97	−14.47	6.40
Average value:	290.6	240.0	2.05	2.44	33.8	27.58	26.57	21.37	−26.3	15.54

Table 7 Design Case 3. Peak Values of system response for HDBI and HDBI+CKBB subjected to moderate ground excitation

	Base		Structural		Isolator		Structural		Actuator	Actuator
	Drift (mm)		Drift (mm)		Work (kJ)		Work (kJ)		Work (kJ)	Power (kW)
		HDBI+		HDBI+		HDBI+		HDBI+	HDBI+	HDBI+
Earthquake	HDBI	CKBB	HDBI	CKBB	HDBI	CKBB	HDBI	CKBB	CKBB	CKBB
1940 El Centro	71.1	30.83	1.74	5.16	22.06	1.46	4.07	14.03	5.43	9.37
1979 El Centro	74.6	23.17	1.57	4.40	11.35	0.86	1.70	12.69	8.36	7.43
1987 Whittier	56.3	28.16	1.74	4.86	6.96	3.49	4.02	4.02	-4.51	18.77
1992 Landers	79.2	53.72	1.67	4.39	24.77	3.10	2.89	17.49	5.09	10.58
Average value:	70.3	33.9	1.68	4.70	16.3	2.59	5.61	12.05	3.59	11.5

Duzce which resulted in a tripling of peak structural drift. Notice, however, that peak values of structural drift under 1999 Duzce are no larger than for the other three ground motion inputs and, in fact, peak drifts in the isolator (although slightly larger) are considerably smaller than for the San Fernando, Northridge and Kobe inputs. We surmise that this anomaly might be due to the extended duration of actuator action – the 90% AI for 1999 Duzce occurs at 12.78 seconds. The maximum

duration of actuator application among the remaining three earthquakes is 7.56 seconds. In all cases, the addition of control reduces the work done by the isolator element, and in 3 out of 4 cases, also work done by the superstructure. Measured across the four ground motion inputs, the average work done and power required by the actuator are 26.29 kJ and 15.55 kW, respectively.

7.3 HDBI and HDBI+CKBB control subject to moderate ground excitations

This design scenario occurs when HDBI and HDBI+CKBB designs are attacked by moderate ground excitations (i.e., a base isolated structure is designed for a severe ground motion, but is subjected to a more likely moderate earthquake.) Table 7 summarizes the peak values of system response quantities generated by the four ground motion inputs. With the exception of the 1971 San Fernando time-history response, system responses for this case study are almost elastic. The isolator yield displacement is 43.39 kN/2,320 kN/m = 18.7 mm. Three of the four records have a displacement ductility of less than 1.65. The exception is the 1971 San Fernando time-history response, which generates a displacement ductility of 2.87. In all cases, peak values of base drift are reduced – the average reduction is 52% – through the addition of CKBB control. As with the other design cases, reductions in base drift are accompanied by increases in structural drift. The addition of CKBB control decreases the amount of work done by the base isolator, but increases work done by the superstructure – on average, work done by the superstructure increases by 349%. The average value of work done by the actuator is 5.85 kJ. The average value of power requirements is 11.54 kW.

7.4 HDBI and HDBI+CKBB control subject to severe ground excitations

The design case 4 scenario occurs when HDBI and HDBI+CKBB designs are attacked by severe ground excitations. Table 7 summarizes the peak values of system response generated by the four ground motions used in this scenario. Figs. 8 through 11 show contours of force-displacement hysteresis in the isolators, time histories work done by the isolators and actuators, and actuator power requirements. With the exception of the 1995 Kobe input, moving from HDBI to HDBI+CKBB reduces the peak base drifts, on average by 24%. Reductions in peak base drift are accompanied by modest increases in the peak structural drift. In all cases, adding CKBB control to HDBI decreased the peak amount of work done by the base isolator. Among the four simulation scenarios, design case 4 places the greatest demand on the actuator performance. The average work

Table 8 Design Case 4. Peak values of system response for HDBI and HDBI+CKBB subjected to moderate severe excitation

	Base		Structural		Isolator		Structural		Actuator	Actuator
	Drift (mm)		Drift (mm)		Work (kJ)		Work (kJ)		Work (kJ)	Power (kW)
		HDBI+		HDBI+		HDBI+		HDBI+	HDBI+	HDBI+
Earthquake	HDBI	CKBB	HDBI	CKBB	HDBI	CKBB	HDBI	CKBB	CKBB	CKBB
1971 San Fernando	424.5	276.00	3.59	4.68	97.23	45.62	38.23	17.77	−62.10	47.54
1994 Northridge	173.0	105.90	2.21	4.26	34.27	23.03	13.78	12.15	−42.90	38.68
1995 Kobe	188.2	220.70	2.80	4.36	104.40	72.28	23.77	20.90	−73.99	52.82
1999 Duzce	68.6	42.53	1.97	5.00	7.10	4.20	5.83	14.20	−36.31	20.63
Average value:	213.6	161.3	2.64	4.57	60.7	36.3	20.4	16.3	−53.8	39.9

done and power required by the actuator are 53.83 kJ and 39.92 kW, respectively.

7.5 Sensitivity of system performance

For design purposes we are interested in quantifying improvements in base isolation system response due to active control, and in identifying elements of system response that are insensitive to systematic variations in ground motion intensity and design methodology. For system responses generated by moderate ground motion attack, aspects of system response (e.g., peak drifts, work done by the isolator, actuator work and power) are of the same order of magnitude in both designs. As required by the base isolation design, lateral drifts are concentrated in the isolator. Peak values of structural drift in the HDBI design (although still small) are almost twice those of the LDBI design – this phenomenon can be simply attributed to the difference in base isolator yield forces and, hence, the ability of the HDBI design to transmit higher shear forces to the main structural

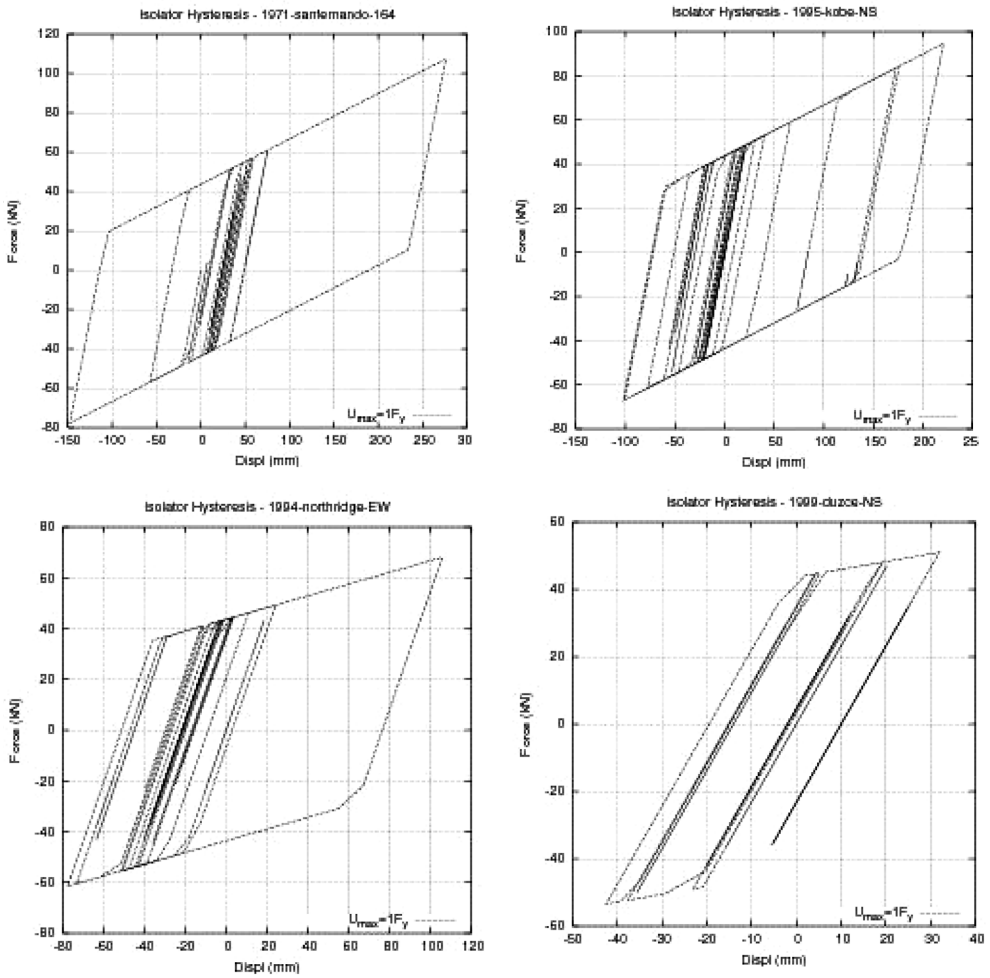

Fig. 8 Design Case 4. HDBI+CKBB design subject to severe ground excitations: 1971 San Fernando, 1994 Northridge, 1995 Kobe, 1999 Duzce. Force-displacement hysteresis curves

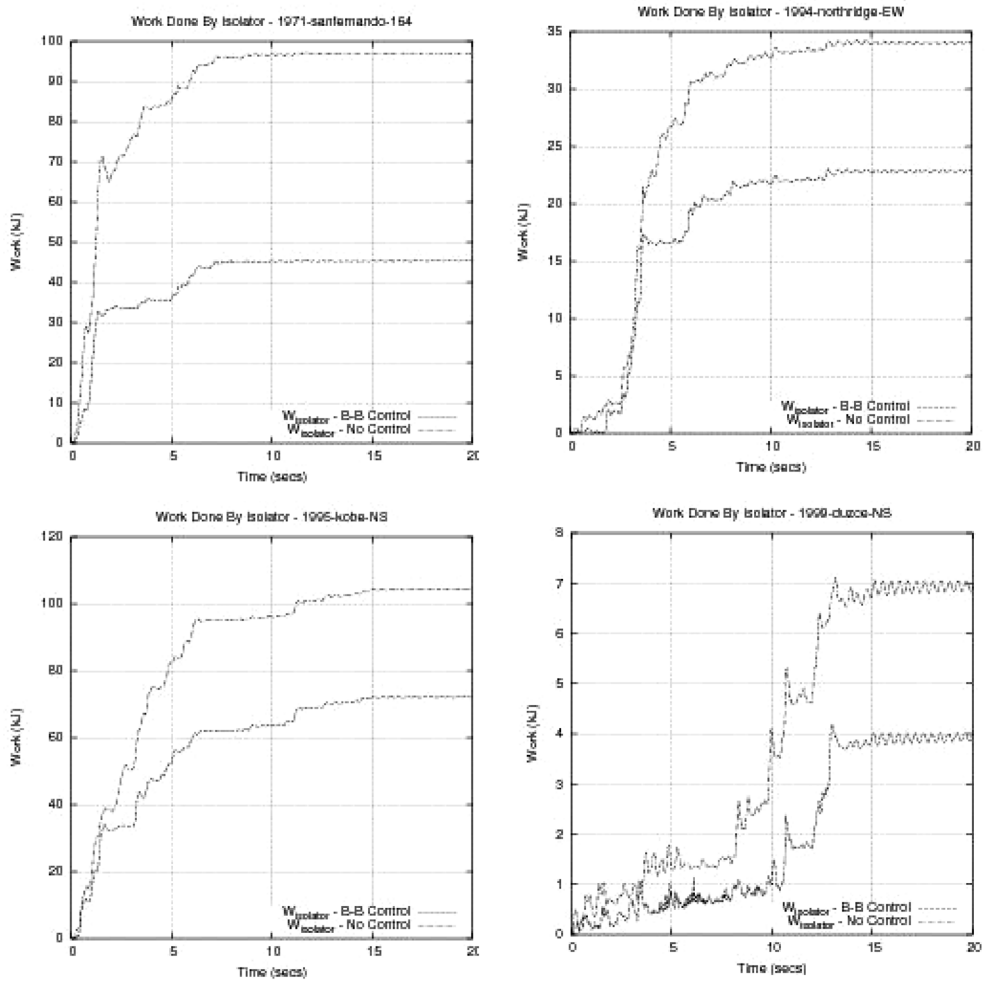

Fig. 9 Design Case 4. HDBI and HDBI+CKBB designs subject to severe ground excitations: 1971 San Fernando, 1994 Northridge, 1995 Kobe, 1999 Duzce. Comparison of base isolator work done (kJ) versus time (sec)

system. In design cases 1 and 3, the magnitude of work done by the actuator is minor and, on the surface, inconsistent. In design case 1 (like design cases 2 and 4), the actuator works to extract small amounts on energy from the system input. Three of the four inputs have actuator work done that is positive, indicating that the actuator feeds input into the system. Drifts are nonetheless reduced by about 50%. Given that peak values of drift under HDBI design are less than half of those generated by LDBI+CKBB and HDBI+CKBB (i.e., design cases 2 and 4), under design scenario 3 the active control should simply be turned off.

As a first step toward understanding this phenomenon, Fig. 12 shows "work done by the actuator" versus "Arias Intensity (m/sec)" for the system responses scaled to moderate and severe ground shaking intensity. Other than noting that "work done by the actuator" is smaller for design cases 2 and 1 than design cases 4 and 3, respectively, it is difficult to identify from Fig. 12 cause-and-effect relationships that have practical meaning. Notice, however, that if we plot "work done by the

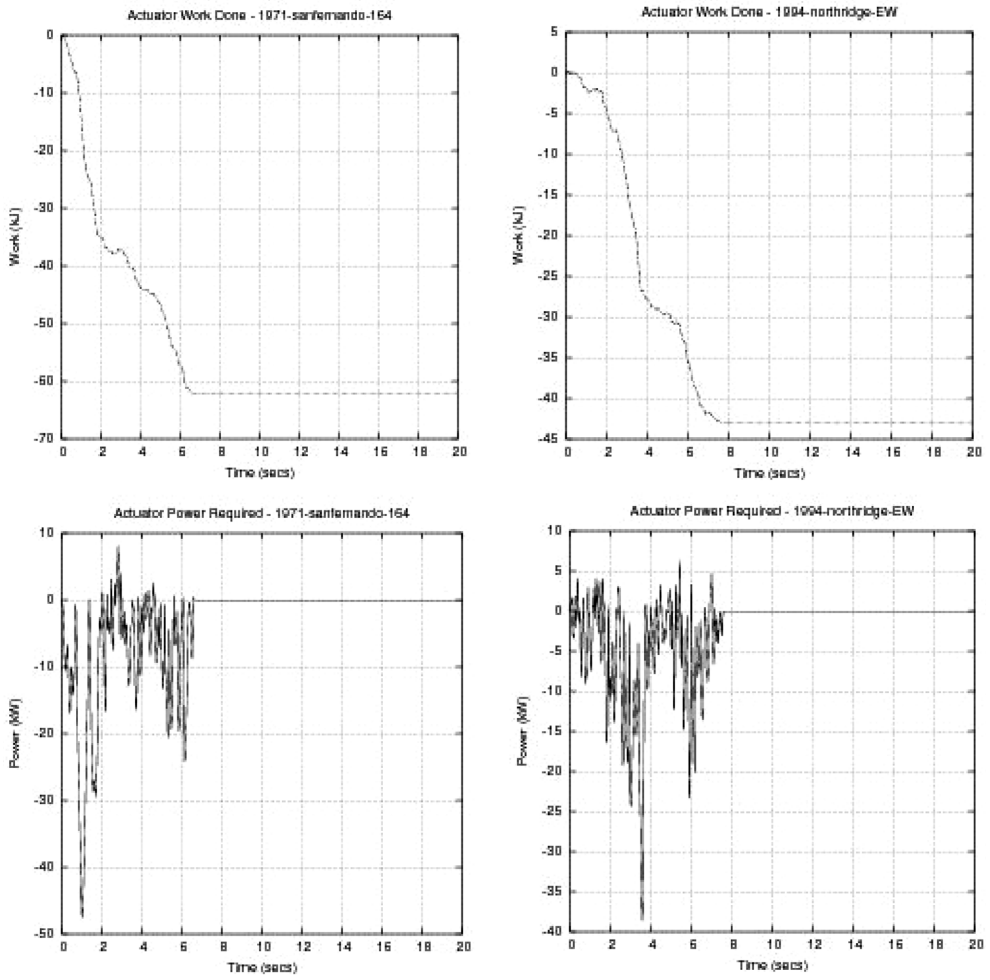

Fig. 10 Design Case 4. HDBI+CKBB design subject to severe ground excitations: 1971 San Fernando, 1994 Northridge. The upper graphs show actuator work done (kJ) versus time (sec). The lower graphs show power requirements (kW) versus time (sec)

actuator" versus "ground motion input energy (AI)/per unit time" the eight system responses for moderate ground shaking separate into two groups. See Fig. 13. The smaller group of three responses corresponds to the three system responses where actuator input energy is positive. We already know from our previous work that the actuator will input energy into the system once the ground motion has stopped (Sebastianelli and Austin 2005). This study suggests that input energy may also be positive for ground motions where "ground motion input energy (AI)/per unit time" is small.

8. Actuator technology assessment

For our LDBI and HDBI models, actuators were modeled with maximum peak forces of 14.46 kN and 43.39 kN, respectively. Peak values of actuator power demand are 24.27 kW and 52.82 kW for

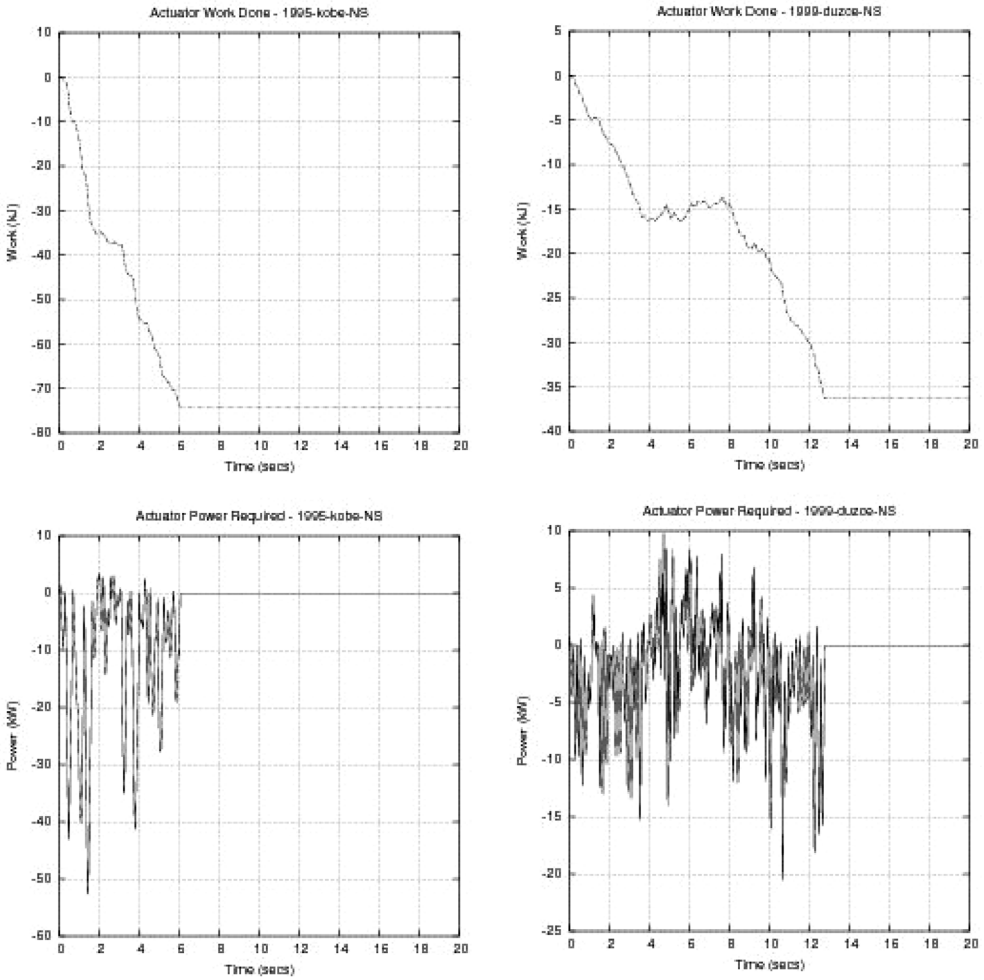

Fig. 11 Design Case 4. HDBI+CKBB design subject to severe ground excitations: 1995 Kobe and 1999 Duzce. The upper graphs show actuator work done (kJ) versus time (sec). The lower graphs show power requirements (kW) versus time (sec)

simulations corresponding to moderate and severe ground motion intensity. Hence, even for this scaled model, it evident that the active control of base isolated structures with actuators generally requires large control forces (tens and possibly hundreds of kilonewtons) with response times on the order of milliseconds.

Two natural questions to ask are: (1) Can present-day actuator technology deliver the range of forces and response times implied by the simulations?, and (2) What implementation difficulties might one face in practice? A summary of key actuator characteristics is shown in Table 9. Hydraulic mechanisms force fluid in or out of a cylinder through an orifice to maintain a certain pressure on the face of a piston head. Dorey and Moore (1996) point out that hydraulic mechanisms can produce forces on the order of meganewtons. However, the disadvantages of hydraulic mechanisms are the requirements for fluid storage system, complex valves and pumps are required to regulate the fluid flow and pressure, and that seals require continuous maintenance. A second

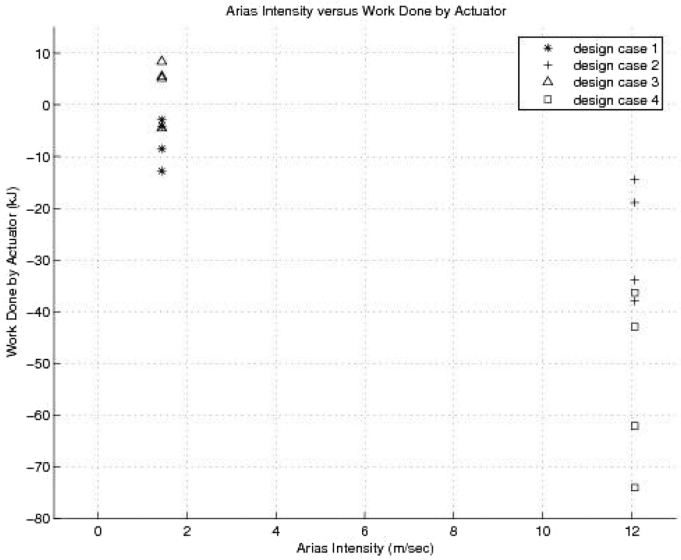

Fig. 12 "Work done by actuator" (kJ) versus "Arias Intensity" (m/sec)

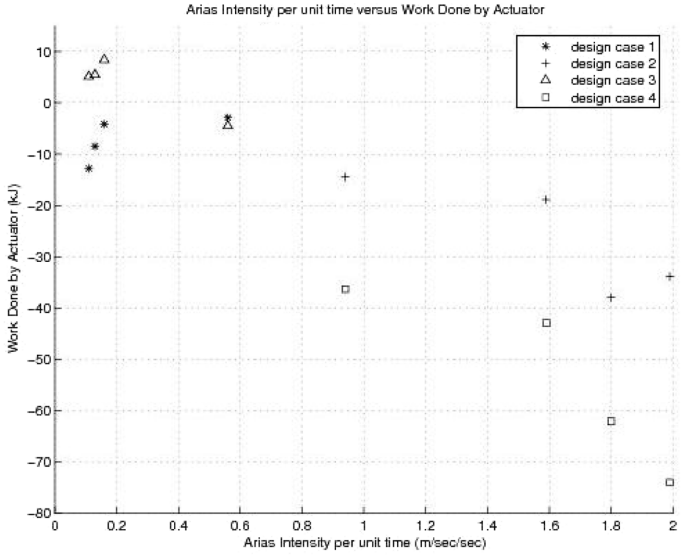

Fig. 13 "Work done by actuator" (kJ) versus "Arias Intensity per unit time" (m/sec/sec)

possibility is electromechanical actuators, which generate force by moving a piston with a gear mechanism that is driven by an electric motor. Electric actuators rated for 600 kN of force are commercial available (see, for example, Raco www.raco.de). Connor (2003) notes, however, that because electro-mechanical actuators are composed of many parts that are in contact with each other, there is a high risk of breakdown.

We therefore conclude that within the simplifying assumptions of this numerical study, yes, present-day actuator technology can deliver forces and response times needed for combined base

isolation and sub-optimal bang-bang control. However, the power demands are not small, and significant challenges may exist in maintaining and verifying operation of such a system over the long term.

9. Conclusions

The conclusions of this study are as follows

1. The numerical experiments indicate that a judicious application of CKBB control can lead to significant improvements in system response compared to those due to base isolation alone. For scenarios of moderate earthquake attack, system responses due to base isolation alone are satisfactory – this is, after all, the purpose of base isolation mechanisms. CKBB control is most effective in countering extreme values of system performance when base isolated systems are subject to severe ground motion attack. From the statistics of performance improvement in peak values of base drift, reductions in energy demands on the base isolator, and actuator power demands it is evident that in all cases, the addition of CKBB control reduces the amount of work done by the base isolator. This observation validates the theoretical formulation for energy-based control.

2. However, is it equally evident that too much control, whether it be through magnitude of the control force or duration of application, can deteriorate performance. Rather than extract energy from the influence of external loads, the situation of "too much" control can feed energy into the system. The latter scenario is most likely to occur after ground motions have ceased and/or during periods of low input energy per unit time. This conclusion points to a strong need for development of a time-adaptive bang-bang control strategy that uses earthquake energy input to navigate trade-offs between work done by the base isolator, superstructure, and actuator.

3. Further work is need to identify trends between "work done by the actuator" and "magnitude of the actuator force" for contours of constant input energy per unit time. If the goal of the active

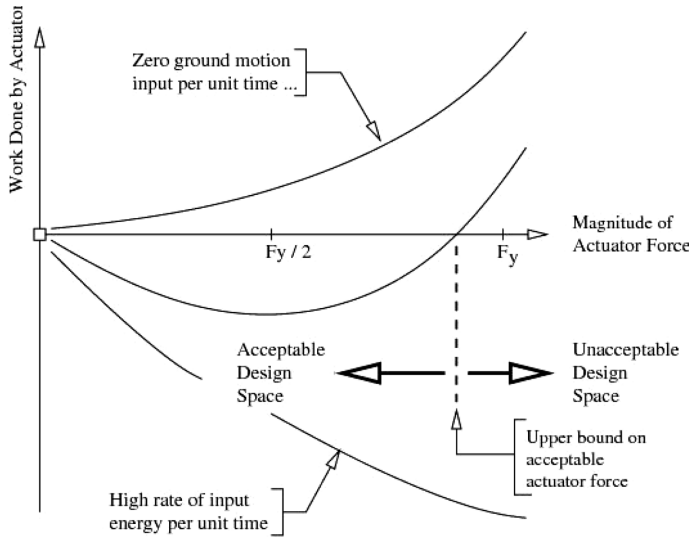

Fig. 14 "Work done by actuator" (kJ) versus "Magnitude of Actuator Force" for Low, Medium, High Contours of Energy Input/per unit time

Table 9 Summary of characteristics of active/semiactive control system actuators

Actuator type	Peak force	Response time	Power requirements
Hydraulic	meganewtons	~10-100 ms	high
Electromechanical	~600 kNs	tenths of secs	high

control mechanism is to extract energy from the system response, while at the same time also decreasing displacements, then we surmise that connectivity among these relationships might be as shown in Fig. 14. Design considerations dictate that no matter how high the rate of energy input becomes, the actuator force should never exceed the lateral yield force of the base isolation system. Appropriate maximum values of actuator force for moderate rates of input energy might be considerably less than the yield force, but would move toward the lateral yield force of the base isolation system as the rate of input energy increases. Conversely, if the actuator force is too small, then the actuator mechanism will be ineffective. Further work is needed to identify the existence of an "upper bound on acceptable actuator force" and to connect this bound to a time-adaptive strategy for bang-bang control.

Acknowledgements

This work was supported in part by a series of Federal Highway Administration Fellowship Grants to Robert Sebastianelli. This support is gratefully acknowledged. The views expressed in this paper are those of the authors, and not necessarily those of the sponsor.

References

American Association of State Highway and Transportation Officials (AASHTO) (1991), *Guide Specifications for Seismic Design.*

Andriono, T. and Carr, A.J. (1991a), "Reduction and distribution of lateral seismic forces on base isolated mutli-storey structures", *Bulletin the New Zealand National Society Earthq. Eng.*, **24**(3), 225-237.

Andriono, T. and Carr, A.J. (1991b), "A simplified earthquake resistant design method for base isolated multistorey buildings", *Bulletin the New Zealand National Society Earthq. Eng.*, **24**(3), 238-250.

Arias, A. (1970), *A Measure of Earthquake Intensity in Seismic Design for Nuclear Power Plants*, MIT Press.

Austin, M.A., Pister, K.S. and Mahin, S.A. (1987), "A methodology for the probabilistic limit states design of earthquake resistant structures", *J. Struct. Div.,* ASCE, **113**(8), 1642-1659.

Austin, M.A., Chen, X.G. and Lin, W.J. (1995), "Aladdin: A computational toolkit for interactive engineering matrix and finite element analysis", *Technical Research Report TR 95-74*, Institute for Systems Research, University of Maryland, College Park, MD 20742.

Austin, M.A., Lin, W.J. and Chen, X.G. (2000), "Structural matrix computations with units", *J. Comput. Civil Eng.,* ASCE, **14**(3), July 2000, 174-182.

Austin, M.A. and Lin, W.J. (2003), "Energy-balance assessment of isolated structures", *J. Eng. Mech.,* ASCE, **130**(3), 347-358.

Bellman, R., Glicksberg, I. and Gross, O. (1956), "On the bang-bang control problem", *Quarterly Applied Math.*, **14**(1), 11-18.

Connor, J.J. (2003), *Introduction to Structural Motion Control,* Pearson Education Inc.

Dorey, A.P. and Moore, J.H. (1996), *Advances in Actuators*, Institute of Physics Publishing, Bristol, England.

Earthquake Engineering Research Center, UC Berkeley (2004), Pacific Earthquake Engineering Research

(PEER) Strong Motion Database, See http://peer.berkeley.edu/smcat/index.html.
Ghobarah, A. and Ali, H.M. (1990), "Seismic design of base-isolated highway bridges utilizing lead-rubber bearings", *Canadian J. Civil Eng.*, **17**, 413-422.
Hall, J.F., Heaton, T.H., Halling, M.W. and Wald, D.J. (1995), "Near-source ground motion and its effects on flexible buildings", *Earthq. Spectra*, **11**(4), 569-605.
Heaton, T.H., Hall, J.F., Wald, D.J. and Halling, M.W. (1995), "Response of high-rise and base-isolated buildings in a hypothetical Mw 7.0 blind thrust earthquake", *Science*, 267.
Housner, G.W. and Bergman, L.A. *et al.* (1997), "Structural control: Past, present, and future", *J. Eng. Mech.*, **123**(9), 897-971.
International Conference of Building Officials (ICBO) (1997), *Earthquake Regulations for Seismic-Isolated Structures: Appendix Chapter 16,* Whittier, California.
Johnson, E.A., Ramallo, J.C., Spencer, B.F., Jr. and Sain, M.K. (1998), "Intelligent base isolation systems", *Proc. of the Second World Conf. on Structural Control.*
Kailaith, T. (1980), *Linear Systems,* Prentice-Hall, London.
Kelly, J.M. and Tsai, H. (1984), "Seismic response of light internal equipment in base isolated structures", *Report No. UCB/SESM-84/17*, Department of Structural Engineering and Structural Mechanics, University of California, Berkeley, CA.
Kelly, J.M., Leitmann, G. and Soldatos, A.G. (1987), "Robust control of base-isolated structures under earthquake excitation", *J. Optimization Theory Appl.*, **53**(2), 159-180.
Lin, W.J. (1997), "Modern computational environments for seismic analysis of highway bridge structures", *Doctoral Dissertation,* Department of Civil Engineering, University of Maryland, College Park, MD 20742.
Mayes, R.L., Buckle, I.G., Kelly, T.R. and Jones, L. (1992), "AASHTO seismic isolation design requirements for highway bridges", *J. Struct. Div.,* ASCE, **118**(1), 284-304.
Naeim, F. and Kelly, J. (1998), *Design of Seismic Isolated Structures*. John Wiley and Sons.
Park, J. and Otsuka, H. (1999), "Optimal yield level of bilinear seismic isolation devices", *Earthq. Eng. Struct. Dyn.*, 28.
Ramallo, J.C., Johnson, E.A. and Spencer, B.F., Jr. (2002), "Smart base isolation systems", *J. Eng. Mech.,* ASCE, **128**(10), 1088-1099.
Reinhorn, A.M., Soong, T.T. and Wen, C.Y. (1987), "Base-isolated structures with active control", *Proc. of Pressure Vessels and Piping (PVP) Conf.*, Vol. PVP-127, 413-420.
Sebastianelli, R. and Austin, M.A. (2005), "Computational assessment of suboptimal bang-bang control strategies for performance-based design of base isolated structures", *ISR Technical Report 2005-89,* Institute for Systems Research, University of Maryland, College Park, MD, p. 72.
Skinner, R.I., Robinson, W.H. and McVerry, G.H. (1993), *An Introduction to Seismic Isolation*. Wiley Publishing, Chichester, England.
Spencer, B.F., Jr. and Nagarajaiah, S. (2003), "State of the art of structural control", *J. Struct. Eng.*, ASCE, 845-856.
Turkington, D.H., Carr, A.J., Cooke, N. and Moss, P.J. (1989a), "Seismic design of bridges on lead-rubber bearings", *J. Struct. Div.,* ASCE, **115**(12), 3000-3016.
Turkington, D.H., Carr, A.J., Cooke, N. and Moss, P.J. (1989b), "Design method for bridges on lead-rubber bearings", *J. Struct. Div.,* ASCE, **115**(12), 3017-3030.
Vision 2000 Committee, *Performance Based Seismic Engineering of Buildings (1995), Volume 1: Interim Recommendations and Conceptual Framework,* Structural Engineers Association of California.
Wang, Y.P. and Liu, C.J. (1994), "Active control of base-isolated structures under strong earthquakes", *Proceeding of the Fifth USA National Conference on Earthquake Engineering*, Vol. 1. Chicago, July 10-14.
Wonham, W.M. and Johnson, C.D. (1964), "Optimmal bang-bang control with quadratic performance index", *J. Basic Eng.*, **86**, 107-115.
Wu, Z. and Soong, T.T. (1996), "Modified bang-bang control law for structural control implementation", *J. Eng. Mech.,* ASCE, **122**(8), 771-777.
Yoshioka, H., Ramallo, J.C. and Spencer, B.F., Jr. (2002), "Smart base isolation strategies employing magnetorheological dampers", *J. Eng. Mech.*, ASCE, **128**(5), 540-551.